

S. KUMAR JAIN<sup>1\*</sup>, Q. MURTAZA<sup>1</sup>, P. SINGH<sup>1</sup>

## MICROSTRUCTURAL AND MECHANICAL CHARACTERIZATION OF WIRE ARC ADDITIVE MANUFACTURED STAINLESS STEEL 316L

Robotic arm technology coupled with Cold metal transfer (CMT) has revolutionized Wire arc additive manufacturing (WAAM), gaining widespread recognition in the aerospace, marine, and automotive sectors. In WAAM, managing residual stress poses challenges due to temperature gradients, phase transformations, and uneven cooling, leading to distortion and potential crack failures. This study is centered on the CMT-assisted fabrication of SS 316L WAAM utilizing a 1.2 mm diameter. It involves a comparative analysis of residual stress, microhardness, ultimate tensile strength, and percentage elongation between SS 316L WAAM, and the results were compared with those of wrought SS 316L. The WAAM sample quantified an average residual stress of 90.73 MPa (compressive), marking an 18% increase compared to the wrought stainless steel's residual stress of 76.68 MPa (compressive). The microhardness profile of the WAAM sample revealed an average value of 269.51 HV0.5, signifying a substantial 4.48% increase over the wrought SS 316L microhardness of 257.94 HV0.5. The WAAM sample's ultimate tensile strength was 577 MPa, 16.56% greater than the wrought SS 316L, having an ultimate tensile strength of 495 MPa, while their respective percentage elongation was 86% and 87%. WAAM demonstrated superior performance in terms of ultimate tensile strength, residual stress, and microhardness.

*Keywords:* SS 316L; WAAM; FESEM; Microhardness; Tensile

### 1. Introduction

The demand for faster manufacturing of components and finished products in recent years has led to gradual shifts in the production infrastructure. Manufacturing technology has advanced significantly, allowing for the formation of complicated metal components with greater ease and at lower cost than was previously possible [1]. The name for this technique is "Additive Manufacturing," and it has been around for some time. Producing in three dimensions with increased material functionality has propelled it to the forefront of manufacturing. WAAM is faster than any other AM process, reducing production time [2]. WAAM is the preferred technology for producing intricate geometries quickly, with high material utilization and low cost. In WAAM operations, the utilization of a high-voltage electric arc as the heat source is fundamental for material deposition. Wire-based feedstock materials are utilized for the deposition process [3]. Industries such as automotive, aerospace, defense, construction, nuclear energy, and biomedical engineering are increasingly adopting WAAM due to its numerous advantages [4,5]. WAAM parts are known for their strength, flexibility, near-net form, cost-

effectiveness, fast manufacturing, and intricate geometries. Wire arc additive manufacturing (WAAM) represents a cutting-edge advancement in the field of manufacturing, as highlighted in the article "New Technologies, Development, and Application [6].

Various welding technologies, including CMT, MIG, TIG, and PAW, can be used for deposition, with TIG and MIG being the most popular. The deposition rate ranges from 2.5 kg/hr to 5 kg/hr to ensure high-quality WAAM [7]. While CMT and GMAW are similar, CMT's droplet transition behavior reduces heat input and improves precision compared to GMAW. The lower heat input of CMT-based WAAM, in comparison to GTAW, has attracted research attention [8]. CMT-based WAAM offers unique advantages, including ultra-low heat input, splash-free droplet transition, a stable arc, precise digital control over material input, and more. These features contribute to the growing interest and application of CMT WAAM in additive manufacturing [9].

Stainless steel 316L stands out for its commendable mechanical properties & less corrosion resistance, attributed to the presence of elements such as Mo, Ni, and Cr [10]. Its remarkable weldability is a result of its higher welding temperature, typically

<sup>1</sup> DELHI TECHNOLOGICAL UNIVERSITY, DEPARTMENT OF MECHANICAL ENGINEERING, DELHI-110042, INDIA

\* Corresponding author: [sudeepjain16@gmail.com](mailto:sudeepjain16@gmail.com)



within the range of 1300°C-1400°C, makes it exceptionally suitable for fusion in Additive Manufacturing. The widespread adoption of SS 316L wires in GMAW is due to its enhanced deposition rate, facilitating the manufacturing of high-strength components with robust mechanical properties [11]. SS 316L characterized as a low carbon austenitic stainless steel, features carbon content less than 0.03 percent by weight [12].

The Wire arc additive manufacturing process emerges as a highly promising tool in the aerospace sector, offering significant potential for the design, production, and maintenance of aircraft and spacecraft. Its simplicity and cost-effectiveness make it a viable alternative to traditional metal additive manufacturing (AM) processes, offering comparable advantages. Its effectiveness with materials such as aluminum and titanium alloys, combined with a high deposition rate and minimal waste, positions WAAM to play a pivotal role in reducing the buy-to-fly ratio in aerospace applications [13]. In their research, Veeman et al. emphasize the significance of titanium in additive manufacturing for nuclear applications. Titanium Grade 9, characterized by high strength and low density, exhibits exceptional corrosion resistance and a favorable strength-to-weight ratio. Predominantly utilized in structural applications, this economically affordable alloy finds widespread acceptance in heat exchangers, storage tanks, columns, fusion reactors, pressure vessels, and piping systems [14].

Despite the immense potential offered by WAAM, it is vital to acknowledge that metal parts crafted through WAAM methods may exhibit imperfections arising from thermal gradients, high temperatures, and rapid cooling. These imperfections encompass issues such as incomplete fusion, porosity, and inclusions within WAAM-produced parts. The pronounced thermal gradients associated with WAAM processes frequently result in the development of substantial residual stress fields. The emergence of issues such as warping, cracking, and distortion stems from this phenomenon, underscoring the critical need to address and mitigate residual stress. This challenge holds paramount importance in industries like nuclear and aerospace technology, where precise dimensional accuracy and resilient mechanical performance are indispensable [15].

The combination of intense local thermal gradients and extremely short interaction durations prompts swift alterations in volume, thereby fostering the development of substantial residual stresses [16]. Compressive residual stress effectively impedes crack growth in welded samples, whereas tensile stress accelerates crack propagation by elevating local stress concentration factors. This mechanism significantly contributes to intergranular stress corrosion cracking [17]. Residual stress assessment involves two primary techniques: destructive & non-destructive methods. Destructive methods entail intentionally removing a small section of the material for investigation. Destructive methods involve intentionally removing a small section of material for investigation. Well-established procedures like hole drilling, contour method, and stripping are categorized as destructive testing, offering a direct approach to acquiring highly accurate data. Non-destructive methods, strategically implemented to combat surface damage challenges, encompass

various techniques like X-ray, magnetic strain, synchrotron radiation, and neutrons. X-ray diffraction (XRD) is particularly highlighted among these methods, offering precise determination of residual stress near material surfaces due to lower X-ray penetration [18]. The XRD  $\sin^2\psi$  stress analysis method commences by conducting a series of XRD scans at specified incident angles ( $\psi$ ) across predefined diffraction angles. After these scans at various incident angles, a pivotal stage involves meticulously verifying the position of the selected diffraction peak. This process necessitates precise measurement of the  $2\theta$  value derived from notably prominent peaks. The Debye-Scherrer ring forms directly due to the diffraction phenomenon, a consequence of applying Bragg's law when X-rays interact with a polycrystalline material [19].

## 2. Materials and methods

WAAM fabrication utilized a robotic system featuring a KuKa robot (Model: KR 8 R1440, Germany) and a CMT source from Fronius (Model: TPS 400i, Austria), a schematic diagram is illustrated in Fig. 1, and the actual setup in Fig. 2(a) & (b). SS 316L material served as both the base and filler wire (1.2 mm diameter). Preliminary trial runs were carried out to establish the optimal process parameters for CMT welding, recognizing the interdependence of current, voltage, and wire feed rate. After a detailed evaluation involving trial runs and a comprehensive literature review, current was selected as the starting parameter, and the remaining two were then determined. The current parameter was chosen after a meticulous trial run and an in-depth exploration of the existing literature. It is essential to emphasize that the welding speed determines the quality of WAAM.

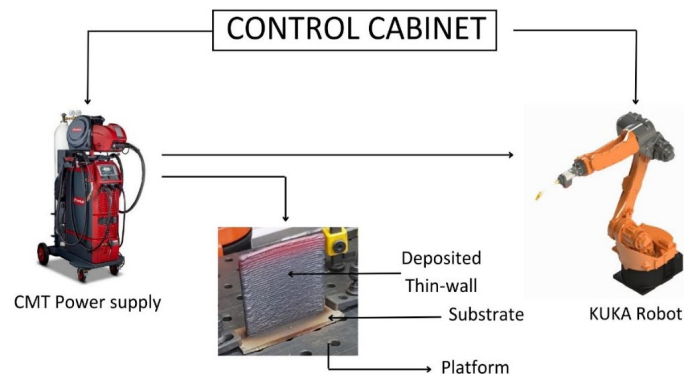


Fig. 1. Schematic diagram of CMT WAAM setup

Comprehensive literature analysis guided the choices related to the shielding gas and its flow rate, emphasizing their significant impact on microstructural characteristics. Specific process parameters for the WAAM sample are outlined in TABLE 1. The chemical compositions (weight%) of filler material are mentioned in TABLE 2.

The fabrication of the WAAM sample involved intricate craftsmanship with a robotic CMT welding source. Before

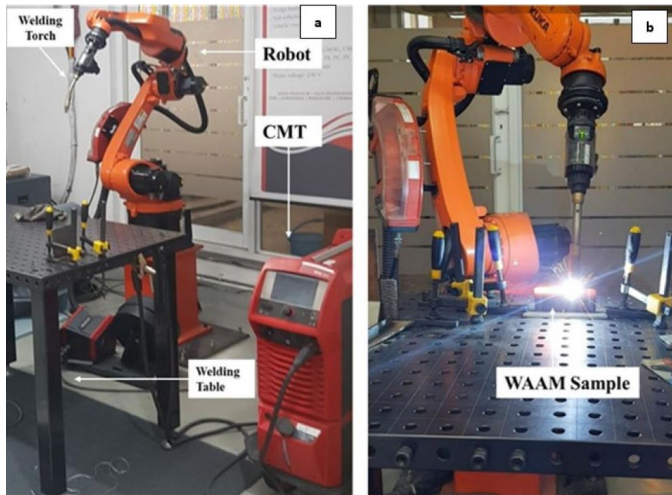


Fig. 2. (a) Robotic-CMT setup (b) WAAM sample fabrication

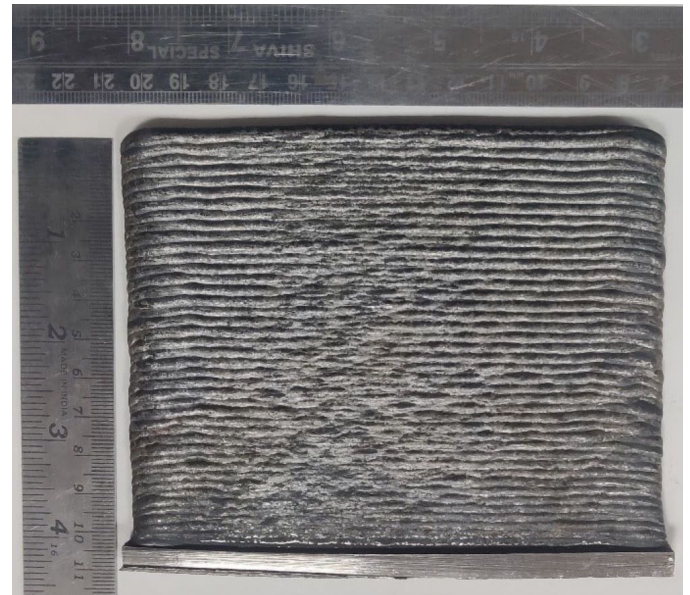


Fig. 3. SS 316L CMT WAAM sample

TABLE 1

Process parameter for CMT-WAAM

Parameters	Value
Current (A)	120
Scanning speed (m/min)	0.5
Voltage (V)	10.6
Wire feed rate (m/min)	2.8
No of layers	40
Contact tip distance (mm)	3.5 mm
Wire diameter (mm)	1.2 mm
Shielding Gas	97% Ar & 3% CO <sub>2</sub>
Gas flow rate (L/min)	15

initiating the welding process, a meticulous cleaning procedure was applied to a  $200 \times 60 \times 6$  mm<sup>3</sup> base. This involved employing a steel wire brush and acetone to effectively remove surface oxides and impurities. The base was securely fastened to the welding table using C-type clamps. Maintaining arc stability and safeguarding the weld bead from impurities were effectively managed by employing a shielding gas as 97% argon (Ar) and 3% carbon dioxide (CO<sub>2</sub>), with an outstanding purity level of 99.99%, consistently supplied at a flow rate 15 liters per minute. The welding torch was accurately positioned with a bevel angle of 90°. Throughout the process, the contact tip distance (CTWD), representing the distance from the nozzle tip to the workpiece, was attentively adjusted to 3.5 mm. Fig. 3 shows the WAAM sample fabricated using robotic CMT welding.

his research entails a thorough assessment of residual stress (RS), microhardness (MH), ultimate tensile strength (UTS), and percentage elongation (PE) for SS 316L WAAM. The preparation involved the precise cutting of three tensile test coupons

adhering to well-defined standards, followed by an intricate polishing procedure to ensure the attainment of precise and reliable results. Tensile testing utilized an INSTRON instrument (Model: 3380, USA) with a controlled cross-head speed of 1 mm/min. From the WAAM sample and wrought 316L, three tensile coupons were meticulously extracted in the transverse (90° perpendicular to welding speed) orientation using wire-cut EDM shown in Fig. 4. The layered structure of WAAM introduced a specific vulnerability in the transverse direction, a notable aspect of the testing. The tensile test specimens, which conformed to the ASTM E8M standard, are depicted in Fig. 4 along with their dimensions.

Vickers microhardness assessments were conducted utilizing a Struers instrument (Model: Duramin-40 M1, make: USA) on the polished samples, per the standards specified in ASTM E384 [20]. The testing parameters included a 500 g load and 10 seconds dwell time. The test encompassed evaluations on SS 316L WAAM at various points vertically, covering from the bottom zone, middle zone, and top zone. This systematic approach aimed to evaluate the uniformity of hardness across the WAAM sample. Additionally, a comparative analysis was conducted on the microhardness of SS 316L WAAM and wrought 316L.

Within the scope of this investigation, residual stress (RS) was carried out using the portable Pulstec  $\mu$ -X360n Full 2D X-ray system (Japan). The adoption of X-ray diffraction (XRD) as the primary methodology for near-surface residual stress measurement was driven by its limited penetration depth, typically around 10  $\mu$ m. The specimens underwent irradiation under meticulously

Chemical composition of SS 316L filler wire material

TABLE 2

Material	Element (Weight %)									
	Cr	Ni	Mo	Mn	C	S	Si	P	Cu	Fe
SS 316L	18.56	11.55	2.53	1.53	0.01	0.01	0.59	0.027	0.17	Rest

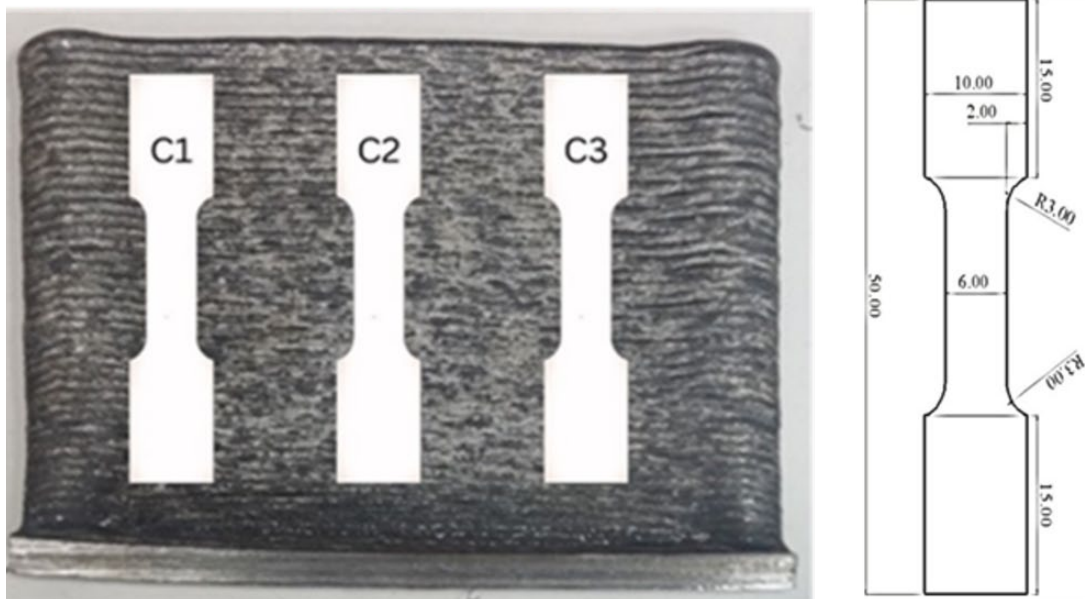


Fig. 4. Tensile coupons from the WAAM sample

defined parameters, involving a beam current of 0.66 mA and voltage of 30 kV. The deliberate adjustment of the X-ray beam incident angle to  $30^\circ$  contributed to the precision of the measurements. The  $\cos \alpha$  technique, ingrained within the  $\mu$ -X360 X-ray Pulstec system, assumes a pivotal role as the foundational approach for calculating in-plane residual stress.

For the microstructural analysis, an Olympus microscope was employed. Initially, the epoxy-mounted samples underwent a stepwise polishing regimen, progressing through emery papers with grit sizes ranging from 400 to 2500. Following this, the polished samples were subjected to a 45-second etching process in Keller's reagent (comprising 2.5%  $\text{HNO}_3$ , 1% HF, 1.5% HCl, and distilled water) before being positioned on the microscope for observation. The same procedure was meticulously followed for the Field Emission Scanning Electron Microscopy (FESEM) analysis, which utilized a Zeiss Gemini 2 (Model: Sigma 300) apparatus operated under high vacuum conditions [21].

### 3. Results and discussion

#### 3.1. Microstructural results

The microstructure analysis of the WAAM sample focused on the central area of its cross-sectional surface. FSEM and optical microscope images (Fig. 5a and 5b, respectively) displayed vertically developed austenite ( $\gamma$ ) and ferrite ( $\delta$ ) along the grain boundaries within the austenite matrix, characterizing the microstructure. Wang et al. observed similar microstructure images of thin-walled SS 316L WAAM [22]. The low heat input in the welding process results from a combination of low current and high gas flow rate. Heat input is directly linked to current and voltage but inversely related to welding speed. Moreover, the elevated gas flow rate accelerates the cooling process, resulting in faster solidification of the sample. The microstructure development follows a ferrite-austenite mode, wherein austenite ( $\gamma$ )

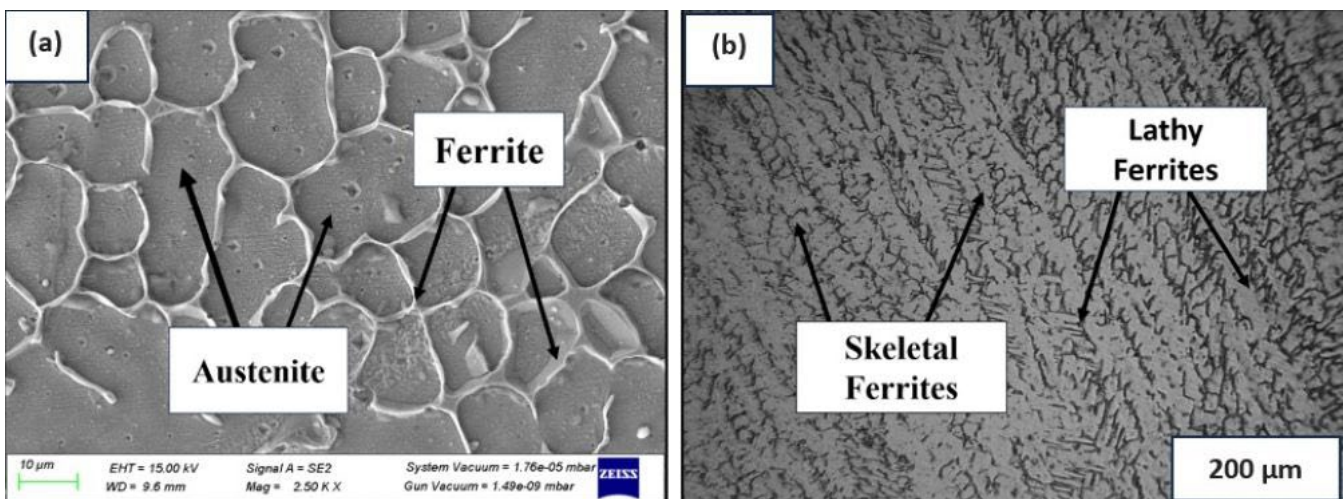


Fig. 5. (a) FESEM image of WAAM sample (b) Optical microscopy of WAAM sample

predominates as the primary phase, while ferrite ( $\delta$ ) is present within the grain boundaries of austenite ( $\gamma$ ). The ferrite exhibits both lathy (parallel structure) and skeletal (dispersed structure) morphologies, as illustrated in Fig. 5b.

### 3.2. Mechanical test results

#### 3.2.1. Tensile test

Fig. 6. presents the stress-strain characteristics derived from tensile testing performed on both SS 316L WAAM and wrought 316L materials. The ultimate tensile strength (UTS) of the AISI 316L WAAM sample measures 577 MPa, which is 16.56% higher than the UTS of wrought 316L, recorded at 495 MPa, as detailed in TABLE 3. Notably, in the context of predominant SS 316L applications where yield strength (YS) is a key consideration, the WAAM sample demonstrates a YS of 284 MPa, a notable 33.34% increase compared to the YS of wrought 316L, which stands at 213 MPa. This emphasizes the potential applicability of the WAAM process in SS 316L applications, particularly in contexts where YS is a crucial parameter. In addition, the comparable percentage elongation values for the WAAM sample (86.5%) and the wrought 316L (87.3%) are almost equal, highlighting the superior ductility inherent in the WAAM sample. This succinctly summarizes the mechanical properties, accentuating the potential utility of the WAAM process in SS 316L applications, especially in situations where both ductility and yield strength assume pivotal roles. Despite closely aligned yield strength values, the CMT WAAM component meets commercial standards, meeting industry requirements for SS 316 L. These results align with the findings reported by Mamedipaka et al. [23].

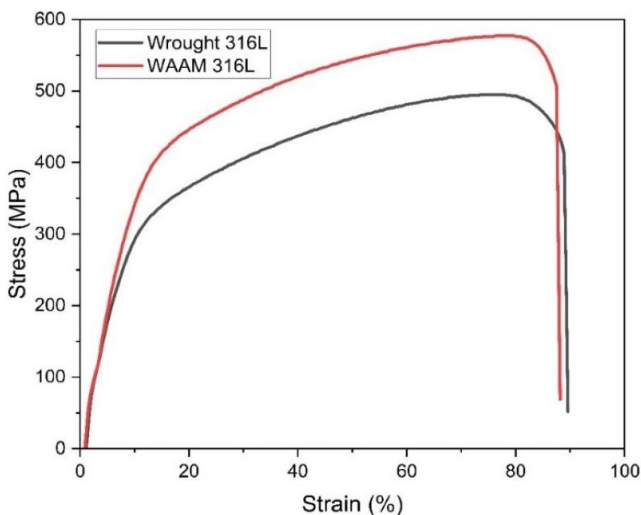


Fig. 6. Stress-Strain Curve of AISI 316L WAAM and Wrought 316L

#### 3.2.2. Microhardness

The research incorporated a meticulous series of microhardness tests at eight specific locations along welding speed direc-

tion at 15 mm intervals, covering the top, middle, and bottom zones of the multi-layered structure as outlined in Fig. 7. The average microhardness values for these zones were 254.87 HV<sub>0.5</sub>, 265.12 HV<sub>0.5</sub>, and 282.56 HV<sub>0.5</sub>, respectively. The results delineate a non-uniform temperature distribution, contributing to a gradual reduction in hardness from the bottom zone to the top zone. The base exhibited the highest recorded hardness at 289.37 HV<sub>0.5</sub>, while the apex displayed the lowest value at 247.56 HV<sub>0.5</sub>. The decrease in hardness from the base to the top is ascribed to significant heat accumulation between layers over time. Notably, the hardness at the joint registered at 287.67 HV<sub>0.5</sub>. TABLE 3 underscores that the average microhardness of SS 316L WAAM measures 269.51 HV<sub>0.5</sub>, presenting a substantial 4.48% increase over the hardness of the wrought 316L, recorded at 257.94 HV<sub>0.5</sub>. The consistent decrease in hardness from the base to the top is a noteworthy pattern. Within the bottom zone, microhardness exhibited a slight increase relative to the top and middle zones, attributed to the initial layer deposition on substrate and consequential heat-affected zone. The microhardness values maintained a steady and uniform pattern across all zones in the fabricated structure, indicating a consistent distribution. This consistent microhardness profile implies the material's resilience against brittle failure [10].

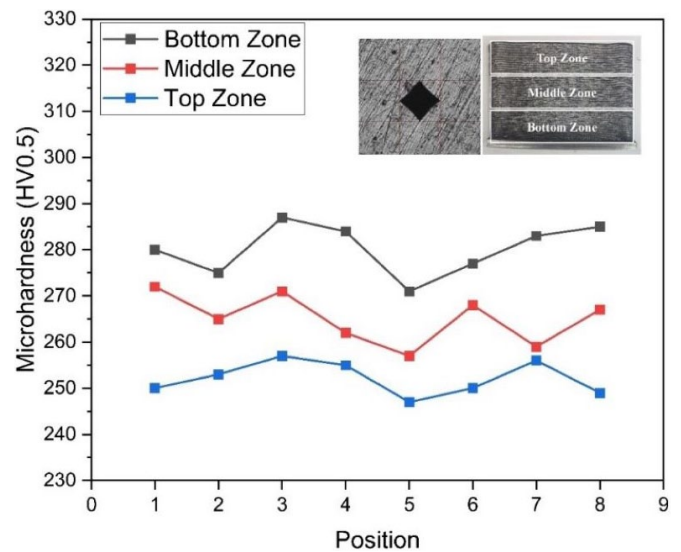


Fig. 7. Microhardness of SS 316L WAAM

#### 3.2.3. Residual stress

Residual stress measurements were systematically undertaken at six specific positions along the vertical axis of the WAAM sample at the bottom zone, middle zone and top zone. The consequential data is effectively presented and elucidated in Fig. 8. Residual stress in the WAAM sample varies from 220.32 MPa (compressive) at the bottom zone near the base to 80.56 MPa (tensile) at the top. The average residual stress across the SS 316L WAAM surface is 90.73 MPa (compressive). The residual stress corresponds with Neto et al findings of compressive residual stresses in SS 304 WAAM components in the transverse

direction. In the interface between WAAM and the base, residual stresses predominantly remained compressive, characterized by a high degree of compressive stress. In the uppermost layer, longitudinal residual stresses transitioned to a tensile nature, attributed to increased constraints on metal shrinkage due to the presence of solidified metal in the longitudinal direction. This phenomenon gives rise to compressive stresses. It is crucial to note that the magnitudes of these residual stresses consistently stay below the material's yield strength [24].

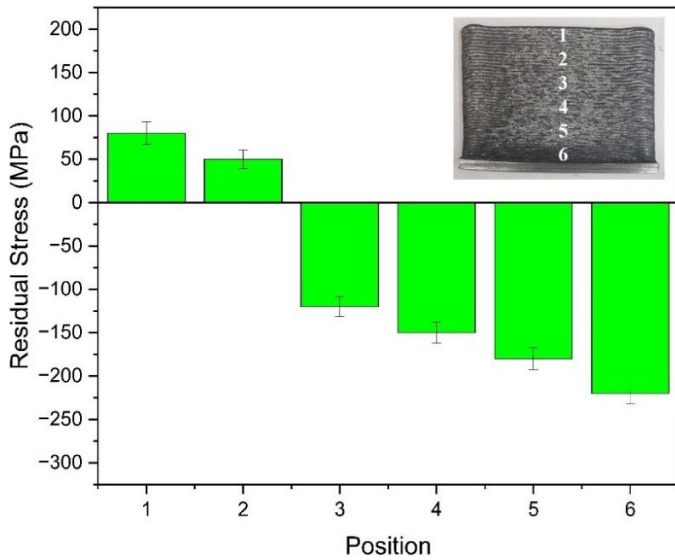


Fig. 8. Residual Stress of SS 316L WAAM

The graphical representation of the DS ring, distortion graph & residual profile is presented, Fig. 9(a) is dedicated to for WAAM sample, Simultaneously, Fig. 9(b) provides data for

wrought 316L. The operational foundation of the  $\cos \alpha$  method relies on continuous D-S rings measured on a two-dimensional detector using a single X-ray source. However, challenges may arise when D-S rings exhibit intermittent characteristics, often due to coarse grain size or limited irradiated areas. Continuous D-S rings, crucial for the  $\cos(\alpha)$  method, necessitate a sufficiently large irradiated area encompassing an ample number of diffracting grains, providing valuable microstructural insights into grain sizes and texture despite potential challenges with coarse grain structures [25].

#### 4. Conclusions

The emergence of robotic CMT WAAM represents a transformative milestone in the landscape of 3D printing for metal components. Renowned for its efficiency and cost-effectiveness, WAAM stands as a particularly suitable method for large-size component manufacturing, owing to its exceptional deposition rates. This research article delves into a comparative analysis of the mechanical properties between the robotic CMT-WAAM process and the wrought 316L are shown in TABLE 3. The study emphasizes four pivotal mechanical properties i.e. ultimate tensile strength (UTS), microhardness (MH), residual stress (RS), and percentage elongation (PE). Based on the findings presented in the research article, Wire Arc Additive Manufacturing (WAAM) emerges as a promising substitute for traditional manufacturing techniques. WAAM exhibits superior performance in terms of both microstructure and mechanical properties when compared to wrought 316L steel. Wire Arc Additive Manufacturing (WAAM) enables the production of components at a lower cost compared to those manufactured through traditional rolling methods. Ad-

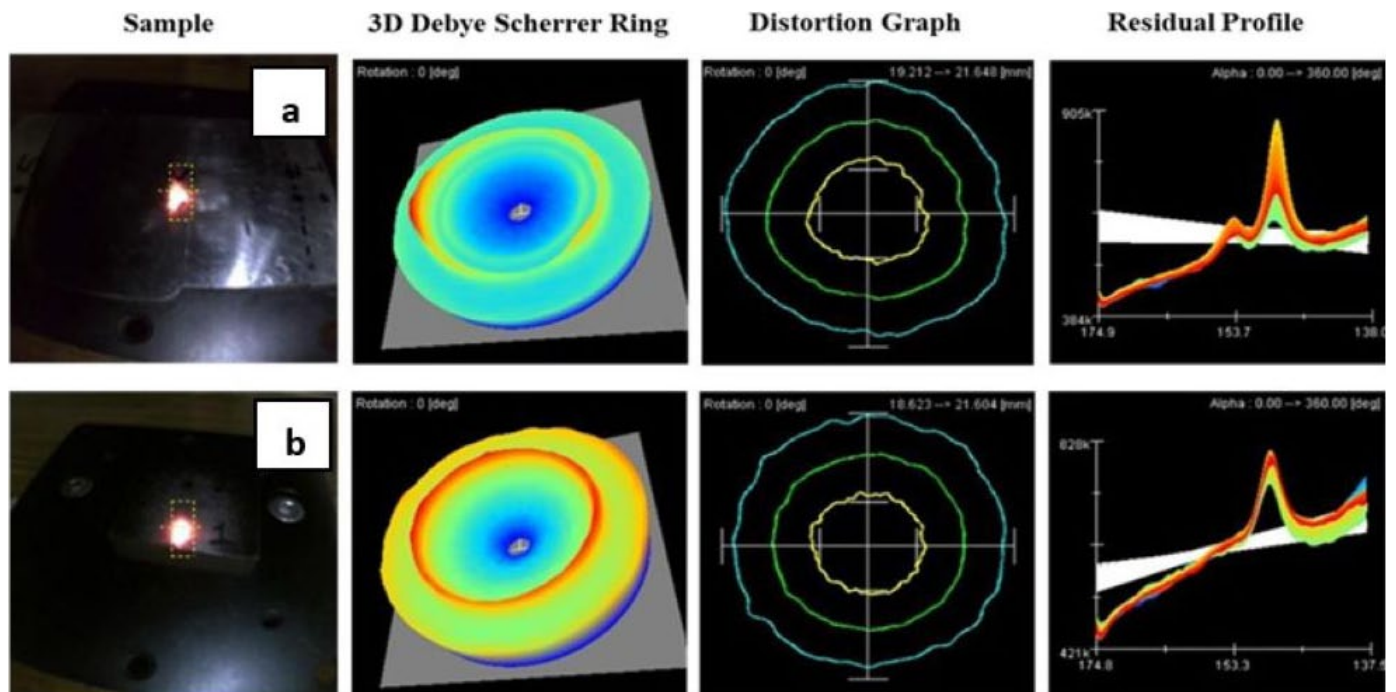


Fig. 9. Sample, 3D D-S Ring, Distortion Graph & Residual Profile of (a) WAAM sample, (b) Wrought 316L

ditionally, WAAM offers the advantage of achieving superior strength, especially in intricate geometries.

The research culminates in the following conclusions.

TABLE 3

Mechanical properties of WAAM sample and wrought 316L

Sample	<sup>1</sup> UTS (MPa)	<sup>2</sup> RS (MPa)	<sup>3</sup> MH (HV 0.5)	PE%
316L WAAM	577	-90.73	269.51	86.2
316L Wrought	495	-76.68	257.94	87.5

<sup>1</sup> UTS in transverse direction (perpendicular to welding speed).  
<sup>2</sup> Microhardness at 8 positions along welding speed direction across bottom, middle and top zone and its average values were considered.  
<sup>3</sup> Residual Stress at 6 positions in transverse direction and the average value was considered.

1. The microstructure development adheres to a ferrite-austenite mode, with austenite ( $\gamma$ ) serving as the primary phase and ferrite ( $\delta$ ) localized within the grain boundaries of austenite ( $\gamma$ ). This dual-phase composition highlights the intricate structural arrangement characteristic of the material's evolution.
2. The WAAM sample exhibited a 16.56% higher UTS than the wrought 316L. Additionally, both the WAAM sample and wrought 316L exhibited comparable yield percentages, with values of 86.2% and 87.5%, respectively. Hence WAAM shows higher strength compared to wrought steel 316L
3. Residual stress assessments revealed higher compressive residual stresses in the WAAM sample compared to the wrought 316L. The average residual stress in the WAAM sample was 90.73 MPa (compressive), indicating an 18.3% increase compared to the wrought with an average residual stress of 76.68 MPa (compressive). The elevated compressive residual strength in WAAM suggests its suitability for components under fatigue loading.
4. The microhardness profile of AISI 316L WAAM averages 269.51 HV<sub>0.5</sub>, showing a 4.48% increase compared to the wrought 316L with a hardness of 257.94 HV<sub>0.5</sub>. The observed variations arise from thermal cycles and microstructural effects, WAAM consistently exhibits higher microhardness than the wrought 316L.

## REFERENCES

- [1] Y. Koli, N. Yuvaraj, S. Aravindan, Vipin, Multi-response mathematical model for optimization of process parameters in CMT welding of dissimilar thickness AA6061-T6 and AA6082-T6 alloys using RSM-GRA coupled with PCA. *Advances in Industrial and Manufacturing Engineering* **2**, 100050 (2021). DOI: <https://doi.org/10.1016/j.aime.2021.100050>
- [2] N. Knezović, A. Topić, *Wire and Arc Additive Manufacturing (WAAM) – A New Advance in Manufacturing BT – New Technologies, Development and Application*. Springer International Publishing (2019).
- [3] R. Rumman, D.A. Lewis, J.Y. Hascoet, J.S. Quinton, Laser Metal Deposition and Wire Arc Additive Manufacturing of Materials: an Overview. *Arch. Metall. Mater.* **64**, 2, 467-473 (2019). DOI: <https://doi.org/10.24425/amm.2019.127561>
- [4] P.S. Gowthaman, Jeyakumar, D. Sarathchandra, Effect of Heat Input on Microstructure and Mechanical Properties of 316L Stainless Steel Fabricated by Wire Arc Additive. *J. Mater. Eng. Perform.* **34**, 13 (2023). DOI: <https://doi.org/10.1007/s11665-023-08312-7>
- [5] A. Chintala, M. Tejaswi Kumar, M. Sathishkumar, N. Arivazhagan, M. Manikandan, Technology Development for Producing Inconel 625 in Aerospace Application Using Wire Arc Additive Manufacturing Process. *J. Mater. Eng. Perform.* **30**, 7, 5333-5341 (2021). DOI: <https://doi.org/10.1007/s11665-021-05781-6>
- [6] P. Steckowicz, P. Pyrzanowski, E. Bulut, Development and implementation of robotized wire arc additive repair of a gas turbine diaphragm. *Bulletin of the Polish Academy of Sciences Technical Sciences* **72**, 2, 1-8 (2024). DOI: <https://doi.org/10.24425/bpasts.2023.147920>
- [7] M. Srivastava, S. Rathee, A. Tiwari, M. Dongre, Wire arc additive manufacturing of metals: A review on processes, materials and their behaviour. *Mater. Chem. Phys.* **294**, 126988 (2022). DOI: <https://doi.org/10.1016/j.matchemphys.2022.126988>
- [8] G. Liu, J. Xiong, External filler wire based GMA-AM process of 2219 aluminum alloy. *Mater. Manuf. Process.* **00**, 1-10 (2020). DOI: <https://doi.org/10.1080/10426914.2020.1779936>
- [9] J. Park, S. H. Lee, Cmt-based wire arc additive manufacturing using 316l stainless steel (2): Solidification map of the multilayer deposit. *Metals (Basel)* **11**, 11 (2021). DOI: <https://doi.org/10.3390/met11111725>
- [10] J. Vora, H. Parmar, R. Chaudhari, S. Khanna, M. Doshi, V. Patel, Experimental investigations on mechanical properties of multilayered structure fabricated by GMAW-based WAAM of SS316L. (2022).
- [11] D.D. Andrea, D. Andrea, C. Hull, Additive Manufacturing Manufacturing of of AISI Stainless Steel: Steel: A. (2023).
- [12] W. Wu, J. Xue, Z. Zhang, P. Yao, Comparative study of 316L depositions by two welding current processes. *Mater. Manuf. Process.* **34**, 13, 1502-1508 (2019). DOI: <https://doi.org/10.1080/10426914.2019.1643473>
- [13] H. Pant, A. Arora, G.S. Gopakumar, U. Chadha, A. Saedi, A. E. Patterson, Applications of wire arc additive manufacturing (WAAM) for aerospace component manufacturing. *Int. J. Adv. Manuf. Technol.* **127**, 11-12, 4995-5011 (2023). DOI: <https://doi.org/10.1007/s00170-023-11623-7>
- [14] D. Veeman, M.K. Subramaniyan, R. Kumar, G. Sriram, M.A. Browne, L. Guo, Additive manufacturing and characterization of titanium wall used in nuclear application. (2023). DOI: <https://doi.org/10.1177/14644207231157578>
- [15] C. Zhang, C. Shen, X. Hua, F. Li, Y. Zhang, Y. Zhu, Influence of wire-arc additive manufacturing path planning strategy on the residual stress status in one single buildup layer. *Int. J. Adv. Manuf. Technol.* **111**, 3-4, 797-806 (2020). DOI: <https://doi.org/10.1007/s00170-020-06178-w>

- [16] M. Srinivas, B.S. Babu, ScienceDirect A Critical Review on Recent Research Methodologies in Additive Manufacturing. *Mater. Today Proc.* **4**, 8, 9049-9059 (2017).  
DOI: <https://doi.org/10.1016/j.matpr.2017.07.258>
- [17] Y. Koli, N. Yuvaraj, S. Aravindan, Vipin, CMT Joining of AA6061-T6 and AA6082-T6 and Examining Mechanical Properties and Microstructural Characterization. *Trans. Indian Inst. Met.* **74**, 2, 313-329 (2021).  
DOI: <https://doi.org/10.1007/s12666-020-02134-0>
- [18] M. Andurkar, T. Suzuki, B.C. Prorok, J. Gahl, S.M. Thompson, Residual Stress Measurements via X-Ray Diffraction Cos- $\alpha$  Method on Various Heat-Treated Inconel 625 Specimens Fabricated via Laser-Powder Bed Fusion. 32nd Int. Solid Free. Fabr. Symp. 1048-1060 (2021).
- [19] M. Braun et al., Mechanical behavior of additively and conventionally manufactured 316L stainless steel plates joined by gas metal arc welding. *J. Mater. Res. Technol.* **24**, 1692-1705 (2023).  
DOI: <https://doi.org/10.1016/j.jmrt.2023.03.080>
- [20] S. Garg, Q. Murtaza, Effect of filler paste's mixing ratio on the properties of Al-64430 dip-brazed joints. *Weld. World* **68**, no. 0123456789 (2024).  
DOI: <https://doi.org/10.1007/s40194-024-01772-y>
- [21] S. Garg, Failure investigation of an elbow pipe used in sewage water treatment facility. *Mater. Corros.*, no. February, 1-8, (2024).  
DOI: <https://doi.org/10.1002/maco.202414336>
- [22] W. Wu, J. Xue, L. Wang, Z. Zhang, Y. Hu, C. Dong, Forming process, microstructure, and mechanical properties of thin-walled 316L stainless steel using speed-cold-welding additive manufacturing. *Metals (Basel)*. **9**, 1, (2019).  
DOI: <https://doi.org/10.3390/met9010109>
- [23] R. Mamedipaka, S. Thapliyal, Data-Driven Model for Predicting Tensile Properties of Wire Arc Additive Manufactured 316L Steels and Its Validation. *J. Mater. Eng. Perform.*, (2023).  
DOI: <https://doi.org/10.1007/s11665-023-08071-5>
- [24] D.M. Neto, M.F. Borges, E.R. Sérgio, F.V. Antunes, Effect of Residual Stresses on Fatigue Crack Growth: A Numerical Study Based on Cumulative Plastic Strain at the Crack Tip. *Materials (Basel)*. **15**, 6 (2022).  
DOI: <https://doi.org/10.3390/ma15062156>
- [25] K. Tanaka, The cosa method for X-ray residual stress measurement using two-dimensional detector. *Mech. Eng. Rev.* **6**, 1, 18-00378-18-00378 (2019).  
DOI: <https://doi.org/10.1299/mer.18-00378>